Applied Mathematical Modelling 146 (2025) 116176

Contents lists available at ScienceDirect

Applied Mathematical Modelling

journal homepage: www.elsevier.com/locate/apm

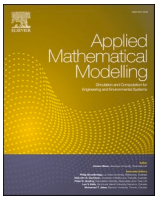

Thermoplastic-virtual integrated model for functionally graded structure at high temperature

Yuan Feng

School of Civil and Environmental Engineering, University of Technology Sydney, Sydney, NSW 2007, Australia

ARTICLE INFO

Keywords:
Thermoplastic
Virtual modelling
Functionally graded structure
Machine learning
Material nonlinearity
Uncertainty quantification

ABSTRACT

The high temperature induced uncertain nonlinear failure behaviour has been one of the critical issues for concurrent composite structures due to the metallic components involved. This paper presents a multivariate coupling framework for combining thermal elastoplastic based mechanical model with efficient virtual modelling technique to investigate the non-deterministic plastic responses of functionally graded structure subject to varied temperature distributions. The position and temperature dependent thermoplastic mechanical properties of functionally graded structure are simulated through the Touloukian and Tamura-Tomota-Ozawa models. The randomness of effective properties of FG structure is applied as random vector into the mechanism algorithm then follow J_2-plasticity with isotropic hardening to exhibit nonlinear behaviour. The coupling framework is achieved by incorporating the random nonlinear responses into the multi-cluster virtual modelling technique and provided with explicit formulation that representing the inherent correlation between the field inputs and yielding outputs. Such that the deformed nonlinear deflection, plastic damage zone, and fragility curves could be directly estimated for the FG structure under various temperature distributions. The coupled thermoplastic-virtual model is validated through two practical numerical applications and the computational accuracy, efficiency, and versatility of the coupled framework ensured the rapid safety evaluation of complex composite system in an uncertain thermal environment.

1. Introduction

As advanced composite materials, functionally graded materials (FGMs) have been widely developed for many high-end applications in various fields, such as aircraft engine blades and piston cylinders in Fig. 1. Most of these devices are often required to operate in high-temperature environments and are generally of high value, with significant secondary losses caused by failure [1,2]. Many accident investigation reports reveal that high-temperature-induced ductile failure is one of the main failure modes for these FGM-made devices [3,4]. When devices are working continuously, the ductile failure of some main parts is difficult to detect due to the lack of significant symptoms [5]. Once plastic deformation occurs, the deformation can increase violently in a short time in a high-temperature environment due to the high-temperature-weakened hardening characteristics [6,7]. This extremely limits the efficient and sufficient intervention of protective measures before failure. Therefore, it is necessary and critical to develop an early-warning system framework that can accurately simulate the thermomechanical responses of FGM structures in high-temperature environments and provide early warnings of areas where plastic failure may occur. This framework should effectively address the following three relevant challenges currently faced.

E-mail address: yuan.feng1@uts.edu.au.

https://doi.org/10.1016/j.apm.2025.116176
Received 2 January 2025; Received in revised form 21 April 2025; Accepted 28 April 2025
Available online 29 April 2025

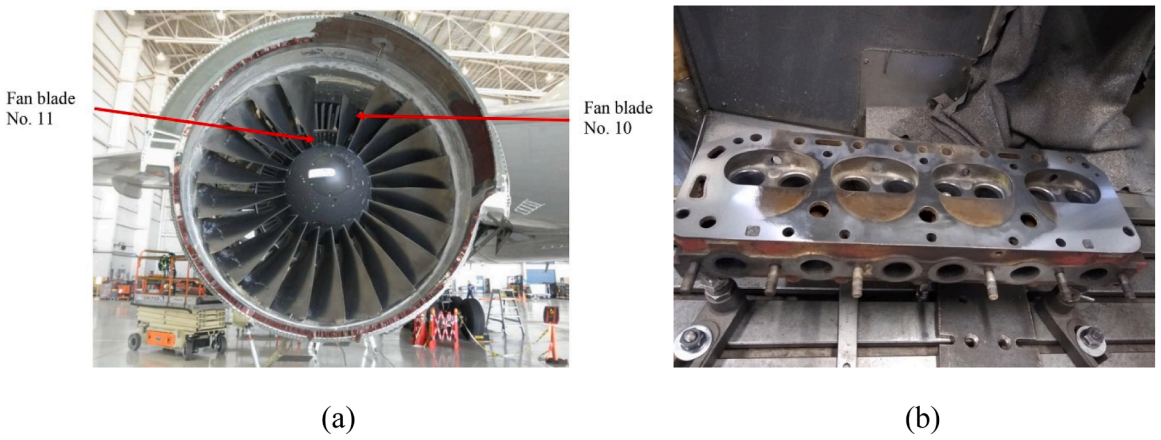

Fig. 1. (a) Ductile failure of blade caused by material defects in the No.2 engine of United Flight 1175; (b) Warping failure of cylinder heads caused by overheating and tremendous pressure.

The first challenge is to develop a thermo-elastic-plastic stability analysis model for complex engineering structures by considering temperature-dependent material properties [8]. Compared to traditional isotropic and composite materials, many FGM-made devices are typically subjected to high-temperature loads with a wide range [9]. Considering the temperature-sensitive material properties, some parts are typically working at their elastic limit and inevitably produce plastic deformation, contributing to a potential ductile failure risk [10]. Therefore, to make a reliable and appropriate FGM structural safety analysis, sufficient consideration of these unavoidable plastic deformations caused by thermomechanical loads and high-temperature-induced material degradation is required [11]. However, most current analysis procedures mainly focus on the buckling analysis of simple structures [12,13], such as single plates and shells, in ambient environments based on analytical [14] and numerical [15] approaches. Some studies have extended to high-temperature environments by simplifying the material properties-temperature relationship, which rarely considers the temperature-dependent characteristics and contributes to unreliable results [16]. In addition, real FGM-made equipment is generally composed of multiple irregular parts, which makes the distribution of stress-strain over the whole equipment impacted by many factors, such as the interaction between each part and the spatiotemporally dependent thermomechanical loads distribution, extremely complex. Therefore, simply focusing on fundamental FGM elements, such as plates and shells, is not enough to accurately reflect the real thermomechanical responses of the whole equipment and also has limited contribution to the design and optimization of FGM structures [17].

In addition, compared with traditional isotropic material-made structures, FGM-made structures generally show more significant inherent uncertainty due to the complexity of manufacturing procedures. These uncertainties, mainly in material properties, should be taken into consideration to ensure the reliability of analysis results. Studies on the uncertainty of FGM systems, including material uncertainties [18], geometrical uncertainties [19], and model uncertainties, are gaining more and more attention. The impact of uncertainties on multiple structural responses has already been investigated [20,21]. Various approaches, such as interval random uncertainty model [22,23], stochastic iso-geometric analysis [24,25], random perturbation-based finite element analysis [26], sampling-based Monte Carlo simulation [27], and first/second order perturbations [28], have been developed to cope with uncertain system parameters. In these studies, MCS-based buckling and stability of FGM structures are one of the main study focuses because of the common ductile-induced buckling failure mode. However, to the author's best knowledge, there are currently no studies focusing on the probabilistic ductile failure analysis of complex FGM structures at extremely high temperatures by considering the inherent uncertainties and temperature-dependent material properties.

The third challenge is improving the efficiency in assessing the safety status of FGM structures after upgrading from a deterministic level to an uncertainty level. Impacted by external environmental factors, the systematic parameters applied to FGM structures, including thermomechanical loads and material properties, fluctuate randomly, which in turn causes continuously changing structural responses [29,30]. These uncertain input systematic parameters and corresponding output responses form a dynamic system. The primary requirements for assessing the safety status of such a dynamic system in real-time are accuracy and efficiency. The safety assessment framework should rapidly and accurately provide the structural responses according to the given latest input parameters, based on which the safety status can ultimately be assessed. Currently, there are two main approaches to obtain output responses: analytical [31] and numerical [32]. The former is only applicable to limited FGM structures with regular shapes, while the latter is generally used for much more complex structures but is time-consuming for large structures, especially when extending to a sampling-based uncertainty analysis [33]. Classical sampling-based MCS is widely used for uncertainty scenarios because of its great applicability and lack of distortion. However, combining numerical and MCS methods to resolve uncertain responses of complex FGM structures is obviously a solution that works in theory but is extremely limited in practical industrial applications due to the huge computational cost. Therefore, designing a more efficient framework is necessary.

To address the above three challenges, this study proposes a real-time safety assessment framework for complex FGM structures by detecting potential ductile failure areas under high-temperature environments. There are three highlights in this framework:

- The Touloukian model, representing temperature-dependent material properties, is integrated into the classical Tamura-Tomota-Ozawa model to simulate the temperature, time, and space-dependent material properties over the whole FGM structure. The randomness of effective properties of the FG structure is applied as a random vector into the mechanism algorithm, then follows J2-plasticity with isotropic hardening to exhibit nonlinear behaviour.
- The inherent uncertainties in temperature-dependent material properties are considered, including Young's modulus, yield strength, hardening parameters, and so on. Random variables that follow specific statistical distributions are used to represent the non-deterministic material properties. Sampling-based MCS is used to obtain the original sample database where the input and output data pairs of each sample are recorded.
- Based on an advanced machine learning algorithm, a virtual model is developed to accelerate the speed of predicting structural responses. Using the original sample dataset as the initial training database, the well-trained virtual model can obtain the explicit function representing the relationship between input parameters and output responses. For any updated input values that exist within the range of the initial training database, this function can always be used to rapidly and accurately predict the corresponding structural responses without any time-consuming numerical simulation procedure. The proposed virtual model has been verified in multiple complex engineering problems, such as nonlinear geometric-material dynamic analysis [34], low [35,36] and high [37] velocity impact analysis, wildfire-induced structural fragility assessment [38] and structural dynamic fracture analysis [39].

To validate the accuracy, efficiency, and robustness of the proposed framework, two practical FGM structures that generally work in high-temperature environments—aircraft engine blades and piston cylinders—are selected as numerical examples to assess their safety status using the proposed framework.

This paper is organized as follows: Sections 2 and 3 introduce the theories used in the study, including the thermoplastic behaviours of functionally graded structures and the variational thermoplastic failure of functionally graded structures. Section 4 demonstrates the virtual modelling technique used to rapidly predict structural responses. Section 5 presents two numerical examples to validate the proposed framework. Section 6 concludes with the highlights of the current work and potential future research directions.

2. Thermoplastic behaviours of functionally graded structure

The functionally graded structure is typically made from two or more types of brittle (e.g., ceramic) and ductile (e.g., metal) materials, with combined mechanical properties transferred continuously along the thickness direction. Such that the volume fractions of ceramic and metal components are formulated as follows.

$$\delta_m(x) = \left(\frac{x}{t} + \frac{1}{2}\right)^n, \quad \delta_c(x) = 1 - \delta_m(x) \tag{1}$$

where δ is the volume fraction of component, x is the location of point ($-t/2 \le x \le t/2$) along the thickness t, n is the power law exponent determining the varying profile of ceramic and metal components.

As the main working condition of high temperature, the functionally graded structure has been designed to resist thermal effects under various mechanical loadings. Thus, it is critical to involve temperature dependent material properties for functionally graded structures to consider more accurate and appropriate structural responses for resilience and reliability evaluation. In this research, the thermal dependent properties are related with the mechanical properties of functionally graded structure by using the Touloukian model [40], which has a generalization expression as follows.

$$\beta(\mathrm{T}) = \beta_0\left(\beta_{-1}\mathrm{T}^{-1} + 1 + \beta_1\mathrm{T} + \beta_2\mathrm{T}^2 + \beta_3\mathrm{T}^3\right) \tag{2}$$

where β(T) is the mechanical properties (e.g., Young's modulus, Poisson's ratio, and yield stress etc.) of functionally graded structure evaluated at temperature T, β_0,β_{-1},β_1,β_2,and β_3 are the thermal coefficients needed to calculate the temperature dependent properties, and the values of those coefficients were experimentally tested and could be referred from [41].

Under high temperature working conditions, plastic properties of functionally graded structure are also varied. For a set thermal environment, the Tamura-Tomota-Ozawa model has been widely used to simulate elastic and plastic material properties of FGM [42]. In this research, considering the inherent thermal effects towards elastoplastic performance of composite, a freshly developed temperature dependent TTO model is reformulated to represent effective thermoplastic properties of functionally graded structure as follows.

$$E(x,\mathrm{T}) = \frac{\delta_m(x)E_m(\mathrm{T})\frac{q+E_c(\mathrm{T})}{q+E_m(\mathrm{T})} + \delta_c(x)E_c(\mathrm{T})}{\delta_m(x)\frac{q+E_c(\mathrm{T})}{q+E_m(\mathrm{T})} + \delta_c(x)} \tag{3}$$

$$\upsilon(x,\mathrm{T}) = \delta_c(x)\,\upsilon_c(\mathrm{T}) + \delta_m(x)\,\upsilon_m(\mathrm{T}) \tag{4}$$

$$\sigma_Y(x,\mathrm{T}) = \sigma_0(\mathrm{T})\left\{\delta_m(x) + \frac{q+E_m(\mathrm{T})}{q+E_c(\mathrm{T})}\frac{E_c(\mathrm{T})}{E_m(\mathrm{T})}[1-\delta_m(x)]\right\} \tag{5}$$

$$\kappa(\boldsymbol{x},\mathrm{T}) = \frac{\delta_m(\boldsymbol{x})\kappa_0(\mathrm{T})\frac{q+E_c(\mathrm{T})}{q+\kappa_0(\mathrm{T})} + \delta_c(\boldsymbol{x})E_c(\mathrm{T})}{\delta_m(\boldsymbol{x})\frac{q+E_c(\mathrm{T})}{q+\kappa_0(\mathrm{T})} + \delta_c(\boldsymbol{x})} \tag{6}$$

where $E(\boldsymbol{x}, \mathrm{T})$ is temperature dependent Young's modulus at temperature T, q is the stress transfer coefficient that needs to be experimentally acquired, in this section, the value of q is selected as 4.5 GPa from [43]. $E_{m,c}(\mathrm{T}), \upsilon_{m,c}(\mathrm{T}), \sigma_0(\mathrm{T})$, and $\kappa_0(\mathrm{T})$ are substitutions of different materials properties $E_{m,c}, \upsilon_{m,c}, \sigma_0$, and κ_0 into Eq. (2), $\upsilon(\boldsymbol{x}, \mathrm{T})$ is the temperature dependent Poisson's ratio, $\sigma_Y(\boldsymbol{x},\mathrm{T})$ is the temperature dependent yield stress, $\kappa(\boldsymbol{x}, \mathrm{T})$ is the temperature dependent hardening parameter for isotropic hardening behaviour of metallic component. It should be noticed that $E(\boldsymbol{x}, \mathrm{T})$ and $\upsilon(\boldsymbol{x}, \mathrm{T})$ are prescribed via mixture rules, and the shear modulus $G(\boldsymbol{x}, \mathrm{T})$ is not independently assigned, but calculated using the relation of $G(\boldsymbol{x},\mathrm{T}) = E(\boldsymbol{x},\mathrm{T})/[1 - 2 \cdot \upsilon(\boldsymbol{x},\mathrm{T})]$. This ensures constitutive behaviour remains consistent with isotropic elasticity theory.

By acquiring effective thermoplastic material properties of functionally graded structures, the corresponding yielding behaviour of the composite is needed to calculate to capture accurate elastoplastic loading paths under various temperatures. Following von-Mises yielding criterion, the critical temperature dependent yielding function of functionally graded structure is defined by:

$$F\big(\sigma(\mathrm{T}), \kappa\big(\varepsilon_p, \mathrm{T}\big)\big) = \sqrt{3J_2(\mathrm{T})/2} - \sigma_0\big(\varepsilon_p, \mathrm{T}\big) = 0 \tag{7}$$

where $J_2(\mathrm{T})$ is the second deviatoric stress invariant at temperature T. Due to the effect of strain hardening the initial yield surface varies at each stage of plastic deformation and the equation of yield surface for a solid undergoing thermo-elasto-plastic deformation is

$$F = F(\sigma, \kappa, \mathrm{T}) \tag{8}$$

After differentiating the F using chain rule of partial differentiation

$$dF = \left(\frac{\partial F}{\partial \sigma}\right)^T d\sigma + \frac{\partial F}{\partial \kappa}\left(\frac{\partial \kappa}{\partial \varepsilon_p}\right)d\varepsilon_p + \frac{\partial F}{\partial T}dT \tag{9}$$

Thus, the total incremental strain combines the incremental parts of elastic strain $\Delta\varepsilon_e$, plastic strain $\Delta\varepsilon_p$, and thermal strain $\Delta\varepsilon_T$ as

$$\Delta\varepsilon = \Delta\varepsilon_e + \Delta\varepsilon_p + \Delta\varepsilon_T \tag{10}$$

By the virtue of Hooke's law, the total incremental stress $\Delta\sigma$ can be written as

$$\Delta\sigma = [\mathbf{D}]\Delta\varepsilon_e = [\mathbf{D}]\big\{\Delta\varepsilon - \big(\Delta\varepsilon_p + \Delta\varepsilon_T\big)\big\} \tag{11}$$

The plastic potential function is assumed to be identical to the yield function as

$$\Delta\varepsilon_p = \frac{\partial F}{\partial \sigma}\Delta\lambda \tag{12}$$

where $\Delta\lambda$ is the plastic multiplier. The component of thermal strains is

$$\Delta\varepsilon_T = \alpha\Delta T \tag{13}$$

where α is the thermal expansion coefficient. Now by substituting Eqs. (12), (13) into Eq. (10), the incremental stress within plastic deformation is achieved as

$$\Delta\sigma = \mathbf{D}_{ep}(\mathrm{T})\Delta\varepsilon \tag{14}$$

where $\mathbf{D}_{ep}(\mathrm{T})$ is the temperature dependent elastoplastic stiffness matrix of functionally graded composite that is expressed as

$$\mathbf{D}_{ep}(\mathrm{T}) = \mathbf{D}(\mathrm{T}) - \mathbf{D}(\mathrm{T})\left[\frac{\partial F(\mathrm{T})}{\partial \sigma(\mathrm{T})}\right]\left[\frac{\partial F(\mathrm{T})}{\partial \sigma(\mathrm{T})}\right]^T \mathbf{D}(\mathrm{T})\left\{\left[\frac{\partial F(\mathrm{T})}{\partial \sigma(\mathrm{T})}\right]^T \mathbf{D}(\mathrm{T})\left[\frac{\partial F(\mathrm{T})}{\partial \sigma(\mathrm{T})}\right] - \frac{1}{\Delta\lambda}\frac{\partial F(\mathrm{T})}{\partial \sigma(\mathrm{T})}d\kappa - \alpha dT\right\}^{-1} \tag{15}$$

where $\mathbf{D}(\mathrm{T})$ is the temperature dependent elastic stiffness matrix of functionally graded composite. Therefore, the thermoplastic behaviour of the concerned structure by using finite element formulation is solved as

$$\left[\int_\Omega \mathbf{B}^T D_{ep}(\mathrm{T})\mathbf{B}d\Omega\right]\Delta\mathbf{d}(\mathrm{T}) = \int_\Omega \mathbf{f}d\Omega - \int_\Omega \mathbf{B}^T\sigma(\mathrm{T})d\Omega \tag{16}$$

where Ω is the whole functionally graded structural domain, $\mathbf{B}$ is material strain-displacement transformation matrix, $\mathbf{f}$ is the external surface traction or distributed loading vector, $\Delta\mathbf{d}(\mathrm{T})$ is the temperature T affected elastoplastic incremental displacement vector.

3. Variational thermoplastic failure of functionally graded structure

3.1. Variational thermoplastic deformation

For practical working conditions, the environmental factors that may cause structural failure could be varied. For instance, the yield strength or hardening parameter of metallic phase of functionally graded structure would be fluctuated with the changing of operating temperatures, which then affect the initial yielding of material prior to the designed bearing capacity. In this research, it is determined that all varying mechanical properties are related with the varying temperature T through the Eq. (2), thus, one unified random vector $\boldsymbol{\theta}(\mathrm{T})$, in which $\theta(\mathrm{T}) : [E(\mathrm{T}), \upsilon(\mathrm{T}), \sigma_0(\mathrm{T}), \kappa(\mathrm{T}), ...]^T$, can be adopted to describe the variational temperature dependent properties of functionally graded structure. Therefore, the corresponding temperature dependent variational yielding function is further defined by:

$$F\{\sigma[\theta(\mathrm{T})], \kappa[\varepsilon_p, \theta(\mathrm{T})]\} = \sqrt{3J_2[\theta(\mathrm{T})]/2} - \sigma_0[\varepsilon_p, \theta(\mathrm{T})] = 0 \tag{17}$$

where the previous deterministic temperature parameter T is replaced with the variational temperature dependent mechanical random vector $\boldsymbol{\theta}(\mathrm{T})$. Also, the incremental plastic strain and stress are updated with the following.

$$\Delta\varepsilon_p[\theta(\mathrm{T})] = \frac{\partial F[\sigma, \kappa, \theta(\mathrm{T})]}{\partial\sigma[\theta(\mathrm{T})]}\Delta\lambda \tag{18}$$

$$\Delta\sigma\{\theta(\mathrm{T})\} = \mathbf{D}_{ep}\{\theta(\mathrm{T})\}\mathbf{B}\Delta\mathbf{u}\{\theta(\mathrm{T})\} \tag{19}$$

Subsequently, the variational thermoplastic deformation $\Delta\mathbf{d}[\boldsymbol{\theta}(\mathrm{T})]$ of functionally graded structure is acquired from:

$$\Delta\mathbf{d}[\theta(\mathrm{T})] = \left\{\int_\Omega \mathbf{f}d\Omega - \int_\Omega \mathbf{B}^T\sigma[\theta(\mathrm{T})]d\Omega\right\} \Big/ \left\{\int_\Omega \mathbf{B}^T D_{ep}[\theta(\mathrm{T})]\mathbf{B}d\Omega\right\} \tag{20}$$

3.2. Plastic failure state of functionally graded structure

The strategy for predicting the ultimate plastic failure state of FGM plates is based on prior research, where nonlinear finite element methods (NFEM) were applied to evaluate the ultimate strength of isotropic homogeneous plates with elastic-perfectly plastic or bilinear elastic-plastic properties [44].

In this research, the FGM plate is subjected to gradually increasing axial compressive loads under different thermal environments. Initially, the plate exhibits recoverable elastic stresses and strains within the elastic range. Once the load exceeds the yield point, plastic deformation begins, resulting in both recoverable elastic strains and irreversible plastic strains. As the load continues to increase, plastic deformation intensifies, eventually causing the plate to lose stiffness entirely and become unstable, culminating in its ultimate failure. The load at this point is referred to as the ultimate plastic failure load and for uncertainties involved cases, variational thermoplastic failure loads of functionally graded structure would be captured. To accurately simulate the plate's load-response behaviour, the analysis is conducted using Newton-Raphson small incremental load steps.

4. S-spline based thermoplastic-virtual model

In this research, the non-deterministic thermoplastic failure analysis of functionally graded structure is achieved by thermoplastic-virtual model based on S-spline kernel. By using a sampling strategy, limited computational efforts are required to construct meta-models that can predict reliable nonlinear responses under various temperature effects for the advanced composites in an efficient manner.

4.1. S-spline polynomial kernel with extended support vector regression

Support Vector Regression (SVR) has demonstrated outstanding capabilities in tackling regression and forecasting tasks [45]. Traditionally, SVR models have relied on Gaussian and polynomial kernel functions. However, these conventional kernels often face challenges when applied to high-dimensional datasets, leading to less accurate predictions. To address this issue, the B-spline polynomial kernel was introduced, offering improved numerical stability in a variety of simulation scenarios. This advancement paved the way for further developments, including enhanced polynomial kernels such as T-splines [46] and P-splines [47]. More recently, the S-spline polynomial kernel has been proposed [48], which offers the advantage of eliminating unwanted control points. The general form of the polynomial kernel function is expressed as:

$$S_{spline}(\zeta_i, \zeta_j) = \sum_{i=1}^{n} P_i B_{2n+1}(\zeta_i - \zeta_j) \tag{21}$$

$$B_n(\zeta_i) = \sum_{r=0}^{i+1} \frac{(-1)^r}{i!} \cdot \frac{(i+1)!}{r!(i+1-r)!} \cdot \left(\zeta_i + \frac{i+1}{2} - r\right)_{\max}^{!} \tag{22}$$

in which P_i is a control point with Cartesian coordinates as:

$$P_i = \varpi_i(x_i, y_i, z_i, 1) \tag{23}$$

The quantity of control points, denoted as n, plays a crucial role in influencing the overall performance of the kernel method. An independent Bayesian optimization approach is employed to efficiently identify the optimal number of control points, ensuring that the kernel function is well-suited for the specific regression task at hand.

As part of the ongoing advancement in SVR methodologies, an innovative variant known as Extended Support Vector Regression (X-SVR) has been introduced to improve the overall quality of training outcomes. X-SVR is particularly chosen for its demonstrated effectiveness in managing highly complex and nonlinear physical systems [35]. One of its key advantages lies in its incorporation of a quadratic ε-insensitive loss function, which contributes to enhanced training stability and improved predictive accuracy. At the outset of the regression procedure, a suitable mapping function is defined to project the input data into a higher-dimensional feature space, facilitating more accurate modelling of nonlinear relationships:

$$x_i = \left[x_{i,1}, x_{i,2}, \cdots, x_{i,n}\right]^T \mapsto \widehat{m}(x_i) = \begin{bmatrix} M(x_1,x_1) & M(x_1,x_2) & \cdots & M(x_1,x_j) \\ M(x_2,x_1) & M(x_2,x_2) & \cdots & M(x_2,x_j) \\ \vdots & \vdots & \ddots & \vdots \\ M(x_j,x_1) & M(x_j,x_1) & \cdots & M(x_j,x_j) \end{bmatrix} = M(x_i) \tag{24}$$

where $\mathbf{M}(x_i)$ denotes the mapping function, $\widehat{m}(x_i)$ is the empirical kernelized vector. In this transformed space, the regression task is formulated as an optimization problem as:

$$\underset{p_x, q_x, \alpha, \vartheta, \hat{\vartheta}}{min} : \frac{\lambda_1}{2}\left(\| p_x \|_2^2 + \| q_x \|_2^2\right) + \lambda_2 e_j^T(p_x + q_x) + \frac{\chi}{2}\left(\vartheta^T\vartheta + \widehat{\vartheta}^T\widehat{\vartheta}\right) \tag{25}$$

where $\vartheta, \widehat{\vartheta}$ denote the redundant constraint parameters; λ_1, λ_2 denote the tuning variables for feature management; χ denotes the penalty coefficient; $\mathbf{p}_x$,$\mathbf{q}_x$ denote the kernelized positive parameters. According to the DrSVR theory, Eq. (25) can then be simplified to a quadratic programming problem as:

$$\begin{aligned} &\min_{y_x, \lambda} : \frac{1}{2}\left(r_x^T \widehat{Q}_x r_x + \alpha^2\right) + \lambda_2 a_x^T c_x \\ &s.t.\left(\widehat{A}_x + I_{4j\times 4j}\right)c_x + \left(\omega I_{4j\times 4j} + \chi\widehat{D}_x\right)\widehat{e}_x + \widehat{g}_x \geq 0_{4j} \end{aligned} \tag{26}$$

$$\begin{aligned} &\underset{\varsigma_x}{min} : \frac{1}{2}\tau_x^T V_x \tau_x - s_x^T \tau_x \\ &s.t. \tau_x \geq 0_{4j} \end{aligned} \tag{27}$$

where the identity matrix is $I_{4j\times 4j}$, the detailed explanation of corresponding matrix vector $\widehat{Q}_x$, $\widehat{A}_x$, $\widehat{D}_x$, a_x^T, $\widehat{e}_x$, V_x, s_x^T and r_x is illustrated in Appendix A. Since the global minimum solution always exists in the optimization problem and is denoted as τ_x^*, the expression of the variables can be written as:

$$c_x = \widehat{Q}_x^{-1}\left(\left(\widehat{A}_x + I_{4j\times 4j}\right)^T \tau_x^* - \zeta_2 a_x\right) \tag{28}$$

$$\chi = \widehat{e}_x^T \widehat{D}_x \tau_x^* \tag{29}$$

Consequently, the governing expression of X-SVR algorithm can be expressed as:

$$\begin{cases} p_x - q_x = c_x(1:j) - c_x(j+1:2j) \\ \widehat{f}(x) = (p_x - q_x)^T \widehat{m}(x) - \widehat{e}_x^T \widehat{D}_x \tau_x^* \end{cases} \tag{30}$$

4.2. S-spline based thermoplastic-virtual modelling of plastic failure

The virtual modelling technique, enhanced by X-SVR with an S-spline polynomial kernel, offers a powerful method for establishing a direct numerical relationship between system variations and high temperature induced nonlinear outputs. This approach eliminates the need to solve complex physical equations. The proposed thermoplastic-virtual framework consists of three primary stages: input setup, virtual model training, and performance evaluation.

In the first stage, system inputs of functionally graded structure are defined, encompassing both deterministic and variational parameters such as geometric configurations, material properties, and boundary conditions. The variational parameters are designed based on specified premises. All input data, including deterministic and non-deterministic parameters, are organized and stored in a database to ensure accessibility for simulations.

In the second stage, repetitive simulations are conducted to generate training data for the virtual model. Thermoplastic nonlinear responses, such as ultimate failure loads under various temperatures, are meticulously extracted from Abaqus simulation results for

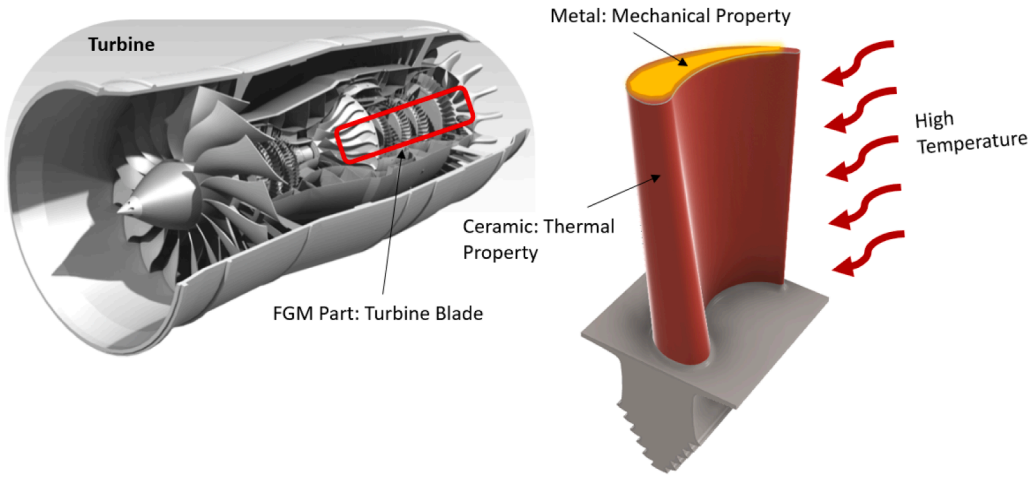

Fig. 2. Numerical example 1: FGM turbine blade.

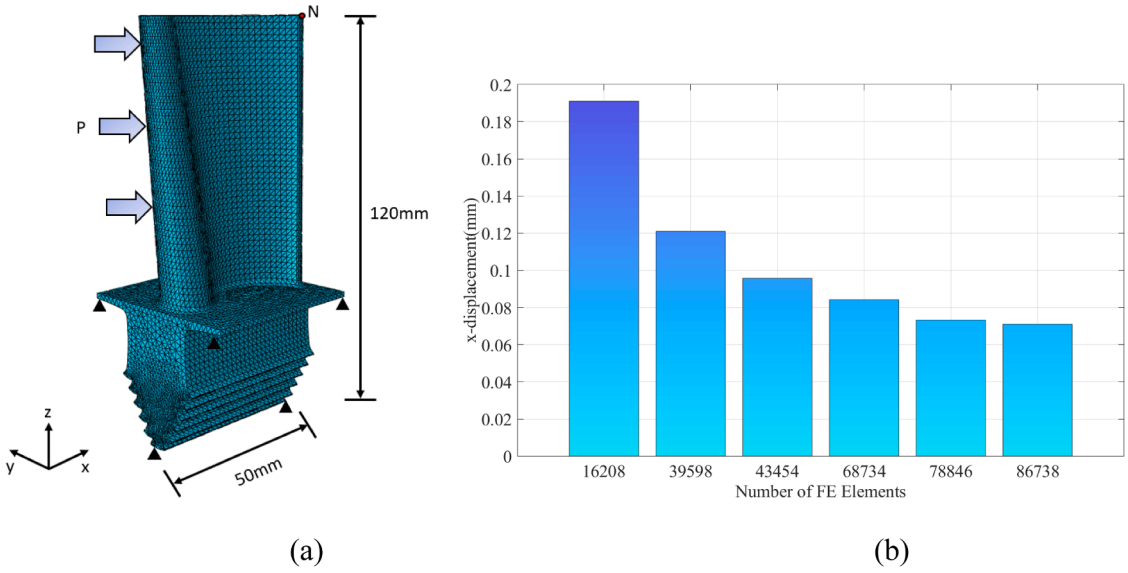

Fig. 3. (a) Adopted mesh condition and (b) mesh convergence study.

each set of input data. These responses, along with the corresponding input variations, are compiled into a comprehensive training dataset.

In the third stage, the X-SVR model with the S-spline kernel establishes a virtual relationship between the inputs and outputs. Once the virtual model is trained, it can predict nonlinear responses of functionally graded structure directly, bypassing the need for solving complex governing equations.

5. Numerical investigation

For the numerical investigations, two cases stem from practical engineering applications are selected to present the random nonlinear responses under varied temperatures, for which including a functionally graded turbine blade and an engine block. The thermoplastic model is adopted for the FGM structures, and the uncertain system information is involved as random vector then analysed by the virtual modelling technique to establish temperature dependent surrogate model. The prediction results of virtual model are rigorously compared with the deterministic simulation approach by using Monte Carlo simulation method, and a series of nonlinear responses are presented to show the effectiveness of the coupled framework. All calculations have been finished on the platform of Intel(R) Xeon(R) Gold 5215 CPU @ 2.5 GHz 10 cores with 192 GB RAM.

Table 1
Variational system properties of the FGM turbine blade [19–23].

System phase	Material property	Distribution type	Mean	Standard deviation
Metal	E_m (GPa)	Normal	200	20
	υ_m	Lognormal	0.27	0.027
	σ_Y (MPa)	Logistic	230	23
	ρ_m (kg/m^3)	Beta	8900	890
	κ_m	Beta	917.5	91.75
	α_m (10^{-6}/°C)	Poisson	9.921	0.9921
Ceramic	E_c (GPa)	Normal	150	15
	υ_c	Lognormal	0.26	0.026
	ρ_c (kg/m^3)	Beta	3960	396
	α_c (10^{-6}/°C)	Poisson	6.826	0.6826
Temperature	T_1 (°C)	Uniform	[350, 450]	
	T_2 (°C)	Uniform	[750, 850]	
	T_3 (°C)	Uniform	[1150, 1250]	

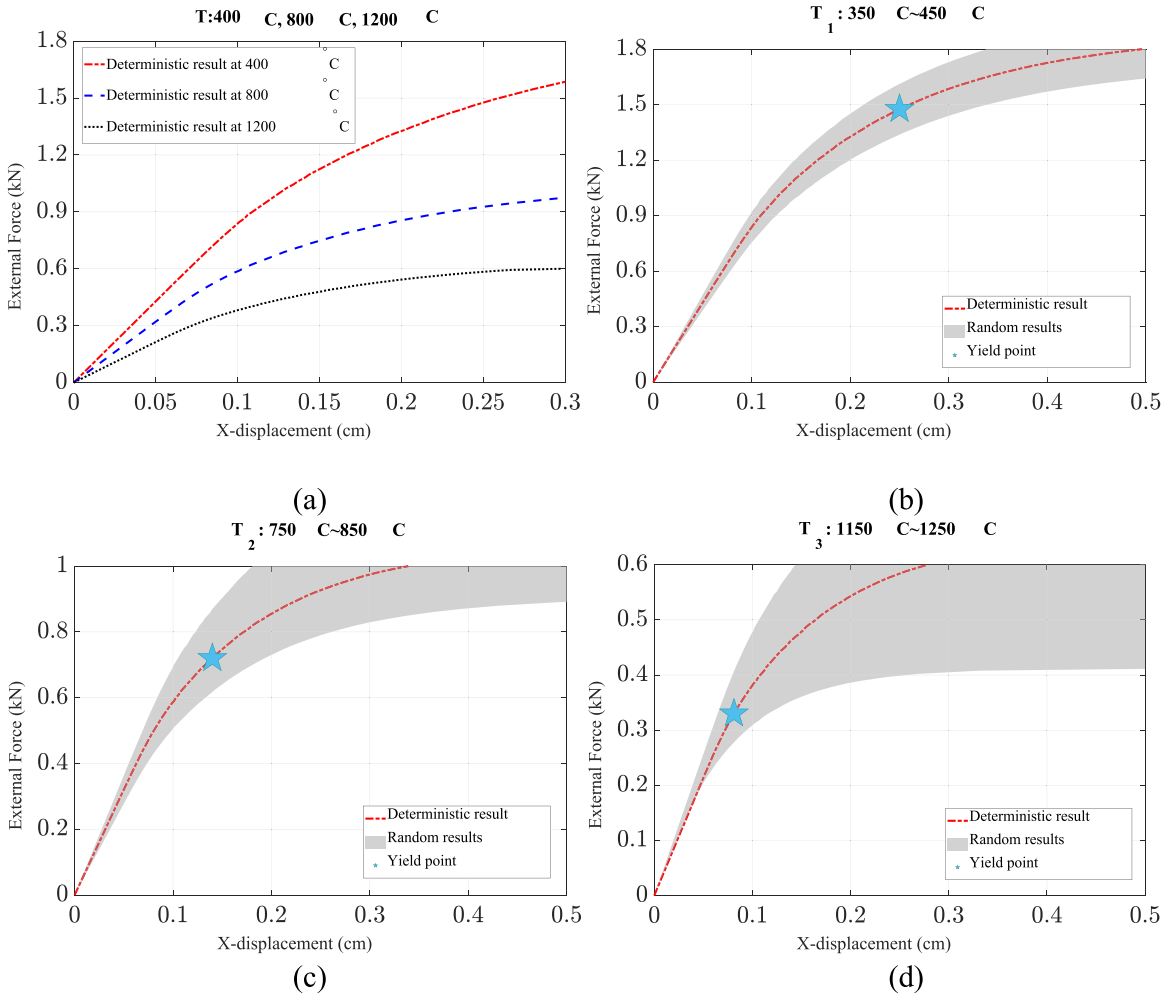

Fig. 4. (a) Deterministic FGM load-displacement curves and random load-displacement curves at (b) 350°~450°, (c) 750°~850°, and (d) 1150°~1250° temperature ranges.

5.1. FGM turbine blade under high temperature

Turbine blade has been considered as essential component in aerospace and aviation engine since last century. However, the failure rates and consequences of turbine blade have been extremely high since the metallic materials made in used may be very vulnerable under engine's frequently encountered high temperature conditions. Thus, in contemporary engineering, FGM made turbine blade has

Table 2
Convergence study of training samples.

Sample	90	120	150	180	210	240	270	300
R^2	0.881	0.912	0.944	0.967	0.983	0.989	0.991	0.992
RMSE	1.356	1.221	1.103	0.887	0.871	0.865	0.861	0.858

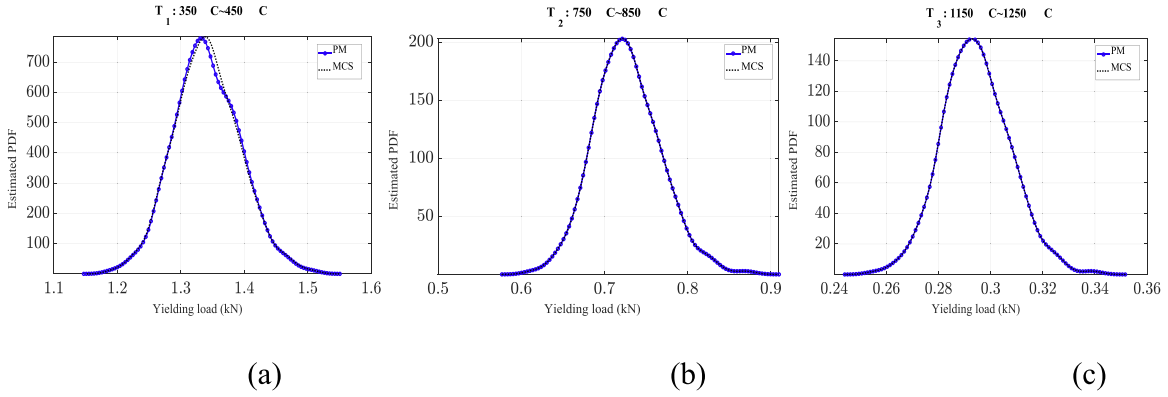

Fig. 5. The estimated PDFs of yielding load from proposed method and MCS results at temperature ranges of (a) 350°~450°, (b) 750°~850°, and (c) 1150°~1250°.

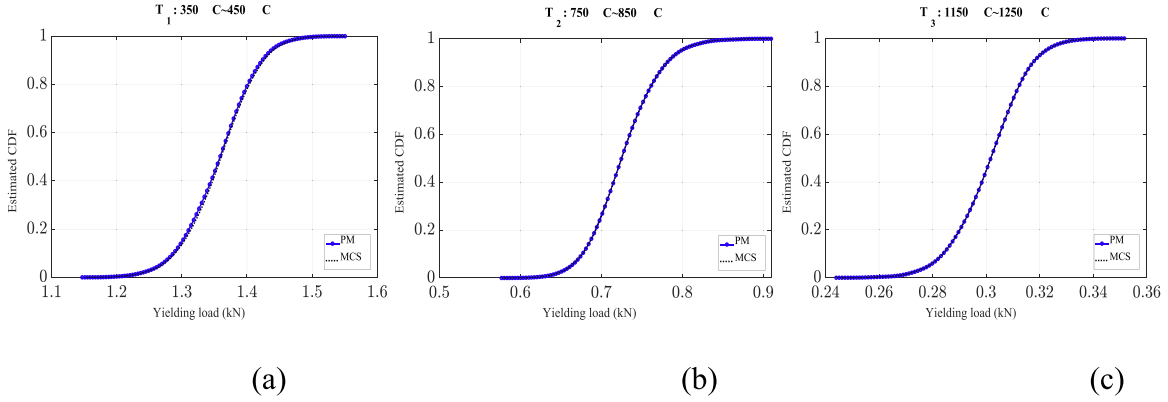

Fig. 6. The estimated CDFs of yielding load from proposed method and MCS results at temperature ranges of (a) 350°~450°, (b) 750°~850°, and (c) 1150°~1250°.

often been implemented in various aerospace, civil, and mechanical fields. In this case, the FGM turbine blade is tested with varied system conditions to quantify the non-deterministic nonlinear response for better safety and reliability assessment. The adopted geometry and physical working condition of FGM turbine blade is shown in Fig. 2. The core of blade is made of metal component then gradually transformed to ceramic component in the outer surface side. The FE mesh convergence study is presented in Fig. 3 and the total number of 86738 tetrahedron elements is adopted to mesh the geometry. The support of turbine blade is fixed and shown with black triangle symbols in Fig. 3 and the blade is working against uniform pressure P along the x-direction with high temperature applied.

In practical engineering, the FGM turbine blade is manufactured with random distributed material properties and working under continuously changing environment. In Table 1, all relevant uncertain information of material and environment has been summarized as random vector $\theta(\mathrm{T}) : [E(\mathrm{T}), \upsilon(\mathrm{T}), \sigma_0(\mathrm{T}), \kappa(\mathrm{T}), ...]^T$ and listed with referable distributions. The metal component deforms plastically with isotropic hardening effects while the ceramic component only considers elastic response. And three uniformly distributed temperature ranges are considered for the FGM blade to simulate varied working temperature scenarios with different structural nonlinear responses. As reference results, the crude 1000 cycles of MCS running would be calculated simultaneously to provide all deterministic results for the uncertain events, comparable results can be found in Fig. 4.

In Fig. 4(a), the deterministic nonlinear responses of FGM turbine blade under three different temperatures from low to high level are shown for understanding purpose and along the curve, the first yielding position representing the structure yields from pure elastic stage to plastic stage is highlighted with a blue star symbol. Then in Fig. 4(b-d), the random elastoplastic responses of FGM blade

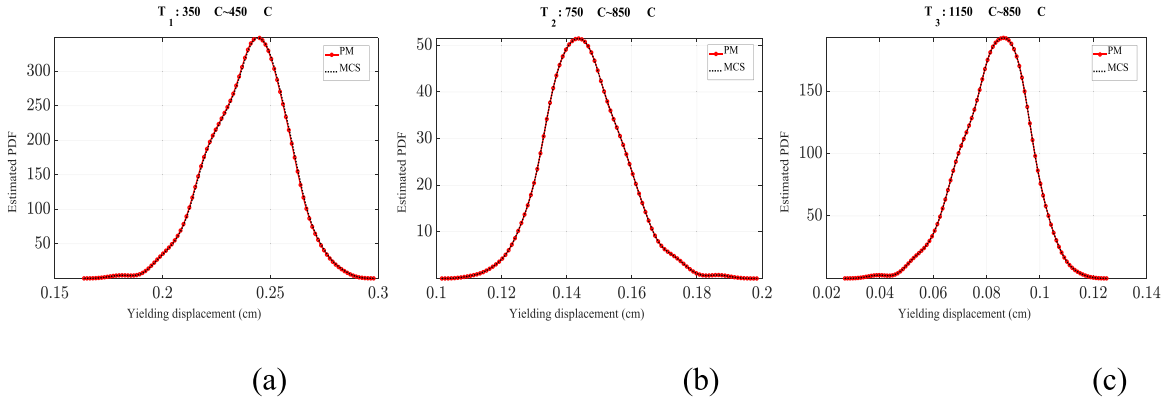

Fig. 7. The estimated PDFs of yielding displacement from proposed method and MCS results at temperature ranges of (a) 350°~450°, (b) 750°~850°, and (c) 1150°~1250°.

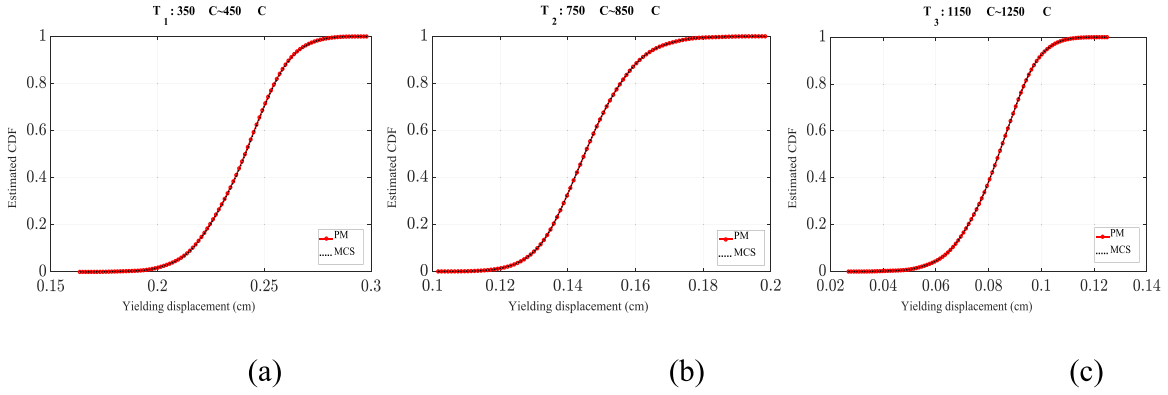

Fig. 8. The estimated PDFs of yielding displacement from proposed method and MCS results at temperature ranges of (a) 350°~450°, (b) 750°~850°, and (c) 1150°~1250°.

Table 3
The estimated moments of yielding load at different temperature ranges.

Temperature range	Moments	Methods	Yielding load	*RE* (%)
T_1	Mean (kN)	PM	1.311	-0.152
		MCS	1.313	-
	Standard deviation	PM	2.124e-03	0.141
		MCS	2.127e-03	-
T_2	Mean (kN)	PM	0.733	-0.543
		MCS	0.737	-
	Standard deviation	PM	3.874e-03	0.180
		MCS	3.881e-03	-
T_3	Mean (kN)	PM	0.298	-1.650
		MCS	0.303	-
	Standard deviation	PM	5.141e-03	-0.214
		MCS	5.152e-03	-

related to the uncertain information listed in Table 1 are provided, and the corresponding initial yielding points in the load-displacement curve are also highlighted with symbols. The yielding points of FGM structure are essential figures to consider the structure has transferred from 'Safe' condition to 'Yield' condition, and the relevant yielding load and yielding displacement can be used to determine the safety limit of concerned composite under different conditions.

The virtual model of FGM turbine blade is constructed with various levels of sample size ranging from 90 to 300 as listed in Table 2. In Table 2, specific mathematical validation figures of R^2 and the RMSE are used to testify the yielding loads between the predicted ones from virtual model and the deterministic ones from MCS results. According to the statistical moments, the sample size of optimal virtual model is selected as 300 for accuracy estimation.

To further illustrate the various yielding conditions of FGM turbine blade under different temperatures, in Figs. 5–8, the relevant

Table 4
The estimated moments of yielding displacement at different temperature ranges.

Temperature range	Moments	Methods	Yielding displacement	*RE* (%)
T_1	Mean (cm)	PM	0.242	0.415
		MCS	0.241	-
	Standard deviation	PM	6.831e-04	0.0293
		MCS	6.833e-04	-
T_2	Mean (cm)	PM	0.153	-1.923
		MCS	0.156	-
	Standard deviation	PM	7.987e-04	1.191
		MCS	7.893e-04	-
T_3	Mean (cm)	PM	0.095	4.396
		MCS	0.091	-
	Standard deviation	PM	9.548e-04	-1.083
		MCS	9.554e-04	-

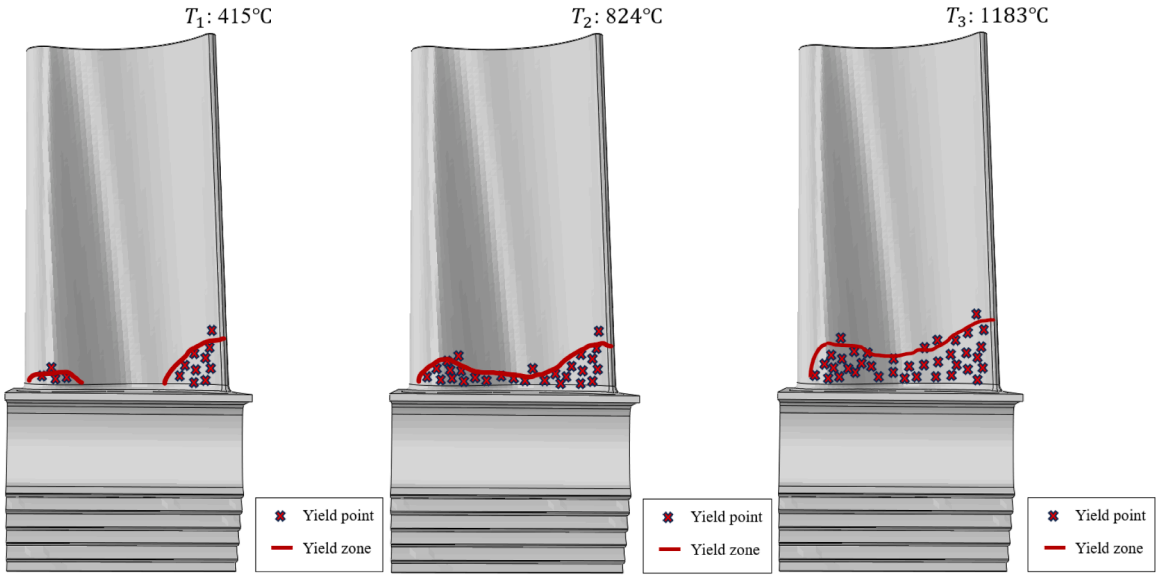

Fig. 9. Predicted yield zone of FGM turbine blade at different temperatures.

probabilistic moments (e.g., probabilistic density function (PDF) and cumulative density function (CDF)) of random yielding loads and yielding displacements have been provided. As shown in Figs. 5–8, with the increment of bearing temperature range, the corresponding yielding capacity of FGM structure is decreased. Specifically, for working temperature around 350^o~450^o, the mean yielding load of structure is 1.35kN and the mean yielding displacement is 0.24cm, but for 1150^o~1250° case, the load is only 0.3kN with the displacement of 0.9cm, which is vulnerable of FGM structure against potential mechanical or structural plastic damage. Moreover, the virtual model established from the proposed method shows great agreement with the deterministic numerical result, however, the computational efforts for predictions of structural yielding information are significantly reduced. The details are: total of 58.3 hours for 300 random samples running, 0.48 hour for virtual model training and establishment, and 2 minutes for yielding load and displacement predictions of FGM turbine blade. All of the calculations are finished on the platform of Intel(R) Xeon(R) Gold 5215 CPU @ 2.5GHz 10 cores with 192GB RAM.

Furthermore, detailed statistical moments about random yielding loads and displacements under three different temperature ranges are provided in Tables 3, 4. It has been clearly shown in the tables that the proposed method results simulate very close to the deterministic MCS responses. The maximum absolute relative error of yielding capacity between two approaches is around 0.15% at temperature range 350^o~450^o, around 0.5% at temperature range 750^o~850^o, and around 1.6% at temperature range 1150^o~1250^o. Similar relative error trend has also been observed for the estimated yielding displacement between two approaches, and it was caused due to the greater deviations of structural responses accumulated from temperature dependent plasticity components. Overall, the accuracy, applicability and efficiency of the proposed framework has been demonstrated through both PDF, CDF plots and statistical moment figures.

With the accumulation of plastic strain in the FGM body, more and more simulation points would be yielded and clustered as yield zones as shown in Fig. 9. The yield zone represents the potential failure region of the concerned structure after initiating with plasticity and could be considered as weak section of advanced structure for further topological optimization and material behaviour

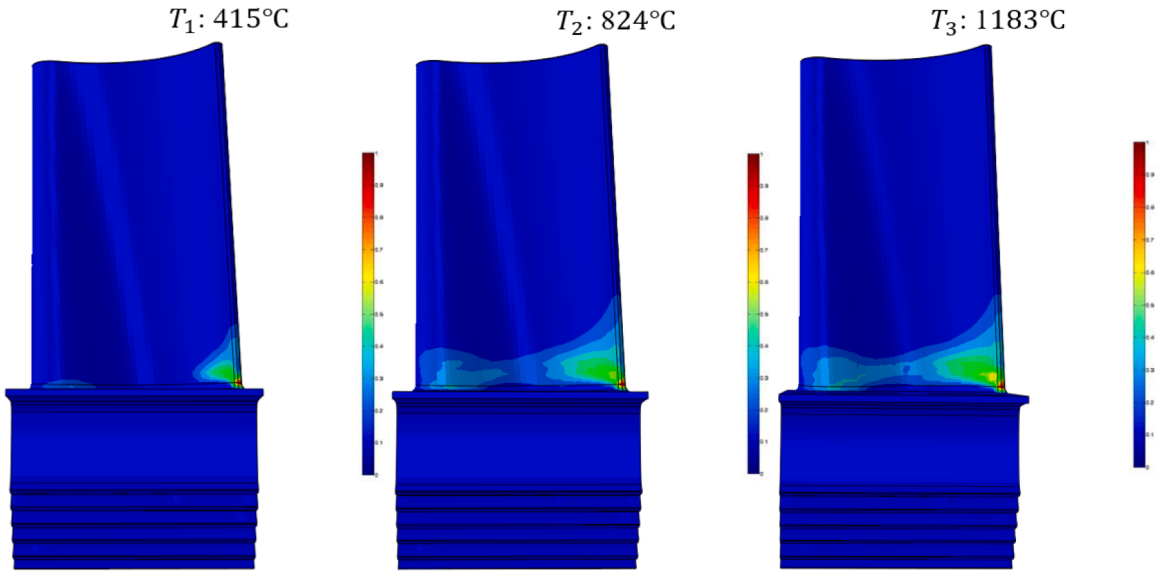

Fig. 10. Deterministic yield zone of FGM turbine blade at different temperatures.

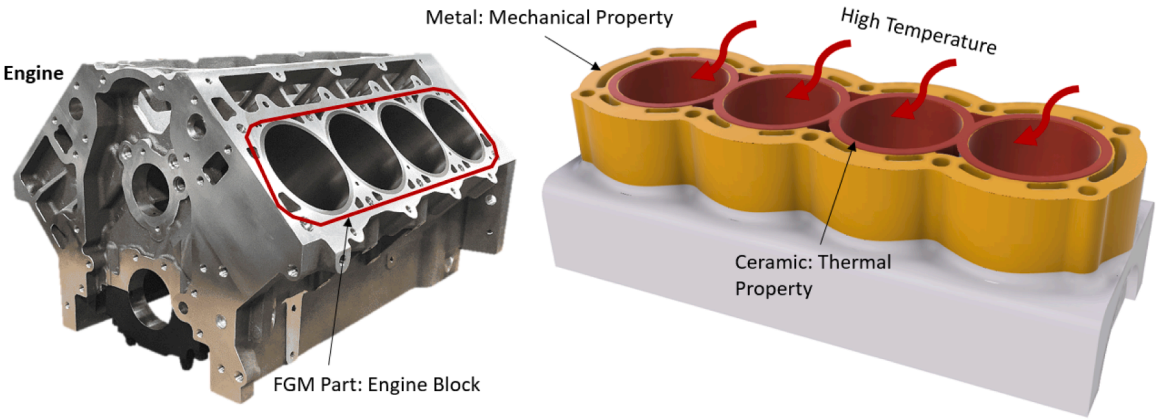

Fig. 11. Numerical example 2: FGM engine block.

strengthens. As shown in Fig. 9, at different randomly assumed temperature levels of 415°, 824° and 1183°, the corresponding yielding points at different locations can be directly estimated through the established virtual model, and the yielding points can be collected as yield zone for FGM turbine blade under different working temperatures. The estimated yield zones have been compared to the deterministic simulation results as shown in Fig. 10, and it can be observed that the estimated yield zones of FGM turbine blade are almost identical with the actual yield regions, but can be predicted in an efficient manner. Therefore, critical structural failure assessment before completely collapse stage can be effectively provided for the designers and engineers to optimize the composite more resilient ones, which highlights the advantages of the proposed coupling framework.

5.2. FGM engine block under high temperature

The second practical application is engine block that has been frequently used in automobile, mechanical, and manufacturing fields. The engine block operates under high temperatures primarily because of the internal combustion process that occurs within it. However, under certain circumstances, factors like the design of the engine block, along with issues of cooling systems, could affect the stability and safety of engine block under long term high temperature effects. Thus, considering the top-tier performance of composite components made for FGM engine block, it ensures that these high temperatures are managed safely and effectively. For this numerical application, the FGM engine block is deformed under various high temperature scenarios, and the nonlinear responses are also recorded from the pure metal made engine block for better comparison purpose. The adopted geometry and physical working condition of FGM engine block is shown in Fig. 11. The core of block is made of ceramic component then gradually transformed to metal component in the outer tube side. The FE mesh convergence study is provided in Fig. 12 and the total number of 11472 tetrahedron

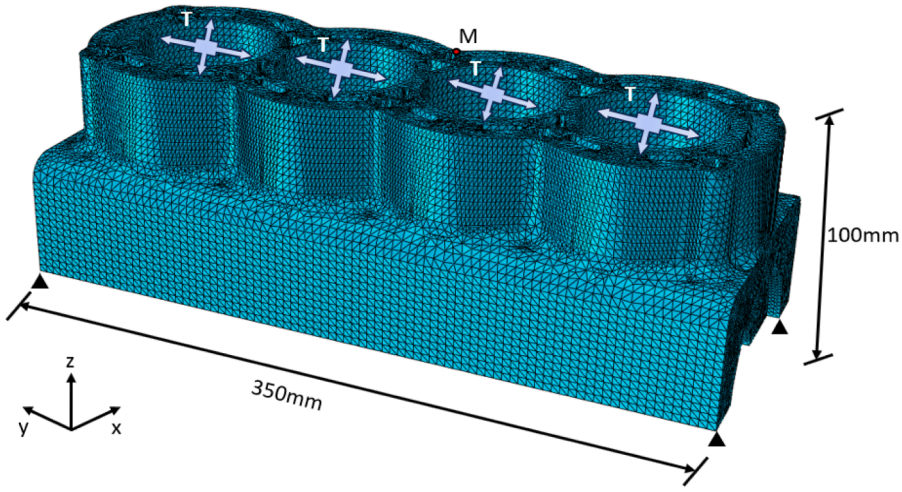

(a)

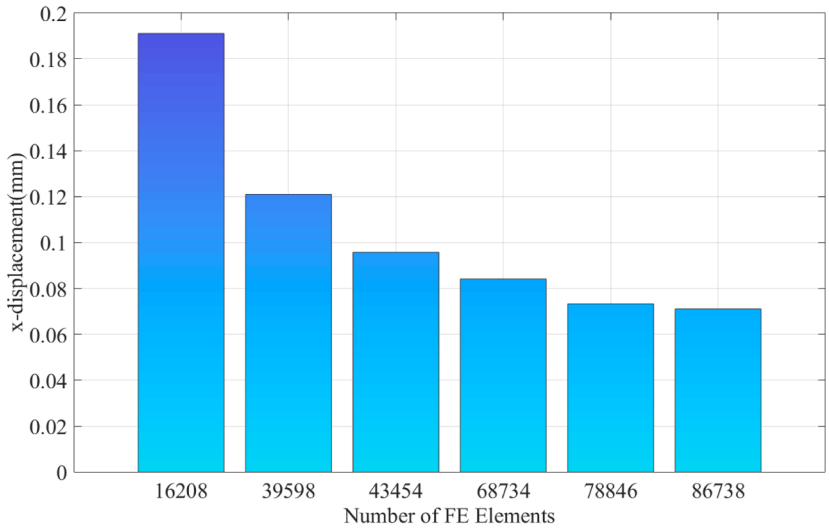

(b)

Fig. 12. (a) Adopted mesh condition and (b) mesh convergence study.

elements is adopted to mesh the geometry. The support of engine block is fixed and shown with black triangle symbols in Fig. 12 and the block is working against uniform distributed pressure P along the internal tube layer with high temperature applied.

The FGM engine block operates in a highly uncertain thermal environment. In Table 5, the relevant uncertain information of material and environment are all considered as random vector $\theta(\mathrm{T}) : [E(\mathrm{T}), \upsilon(\mathrm{T}), \sigma_0(\mathrm{T}), \kappa(\mathrm{T}), ...]^T$ with the corresponding distribution parameters. The metal component deforms plastically with isotropic hardening effects while the ceramic component only considers elastic response. As comparison, for the second case, both FGM component and pure metal component are analysed with three uniformly distributed temperature ranges to investigate different nonlinear behaviours between the traditional homogenous ones and advanced composite ones. As reference results, the crude 1000 cycles of MCS running for two types of material would be calculated simultaneously to provide all deterministic results for the uncertain events, comparable results can be found in Fig. 13.

By collecting all random yielding points information as training dataset, the virtual model of both FGM engine block and pure metal are tested with different levels of sample size as listed in Table 6. In Table 6, at the sizes of 240 and 270, the R^2 and the RMSE of both materials present converged trend to develop stable surrogate models, respectively. Thus, the optimal training size for FGM engine block and pure metal structure is selected as 270 for conservative purpose.

Observed from Fig. 13, it is evident that the high temperature induced nonlinear performance of FGM engine block exhibit clear

Table 5
Variational system properties of the FGM engine block [19–23].

System phase	Material property	Distribution type	Mean	Standard deviation
Metal	E_m (GPa)	Lognormal	220	22
	υ_m	Normal	0.24	0.024
	σ_Y (MPa)	Beta	210	21
	κ_m	Logistic	823.5	82.35
	ρ_m (kg/m^3)	Normal	6500	650
	α_m (10^{-6}/°C)	Beta	7.642	0.07462
Ceramic	E_c (GPa)	Lognormal	160	16
	υ_c	Normal	0.23	0.023
	ρ_c (kg/m^3)	Normal	3250	325
	α_c (10^{-6}/°C)	Beta	5.112	0.5112
Temperature	T_1 (°C)	Uniform	[450, 550]	
	T_2 (°C)	Uniform	[950, 1050]	
	T_3 (°C)	Uniform	[1450, 1550]	

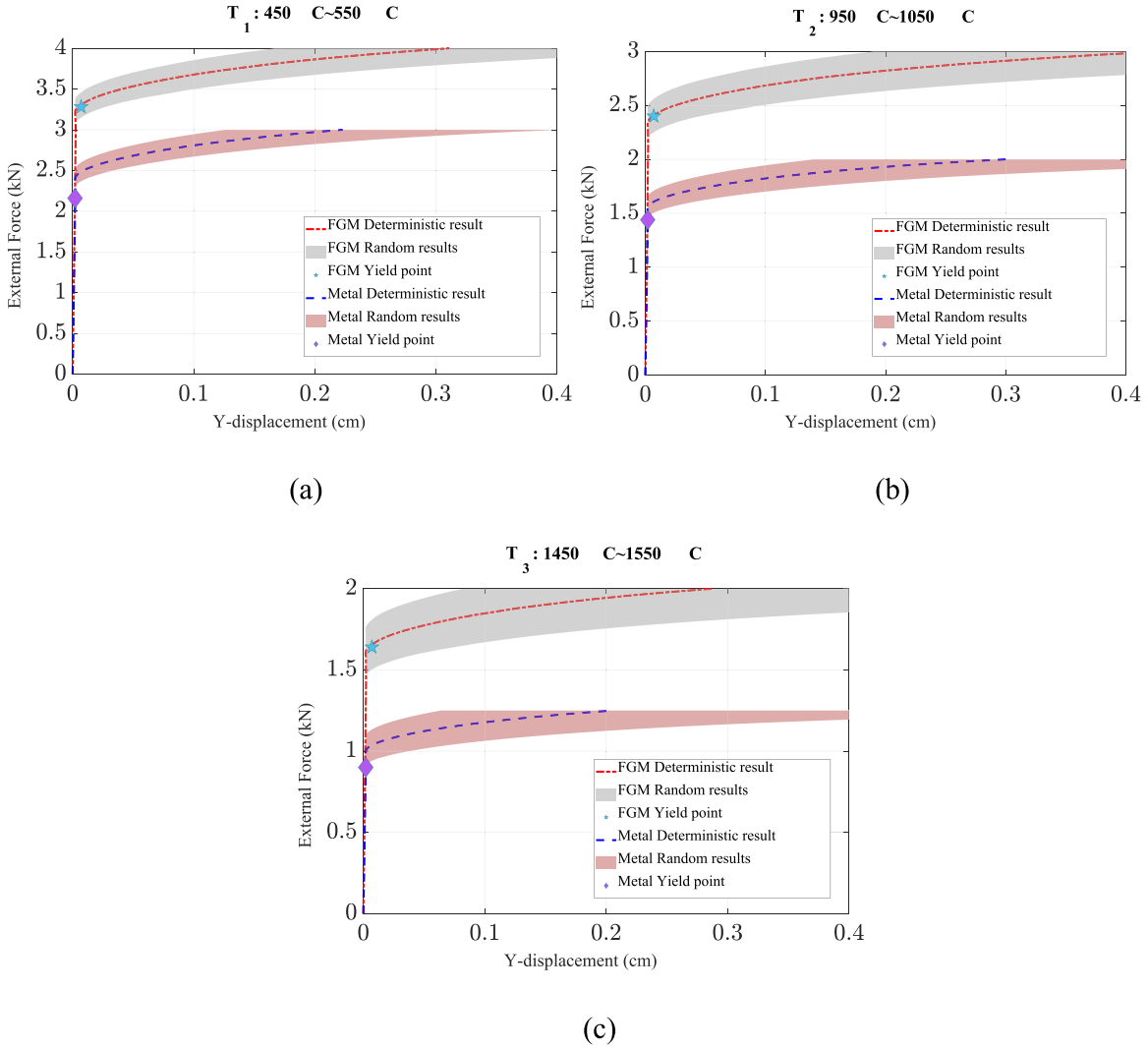

Fig. 13. Random load-displacement curves at (a) 450°~550°, (b) 950°~1050°, and (c) 1450°~1550° temperature ranges.

differences with the pure metal block. To better demonstrate the different yielding information of FGM block and metal block under different temperatures, the PDFs and CDFs of random yielding loads and yielding displacements are provided in Figs. 14–17. From Figs. 14 to 17, the yielding capacity of FGM engine block shows greater values than pure metal block among three temperature

Table 6
Convergence study of training samples.

Material	Sample size	90	120	150	180	210	240	270
FGM	R^2	0.932	0.945	0.966	0.987	0.988	0.992	0.992
	RMSE	0.423	0.341	0.312	0.272	0.226	0.205	0.203
Metal	R^2	0.901	0.932	0.954	0.967	0.978	0.989	0.991
	RMSE	0.656	0.521	0.403	0.387	0.371	0.365	0.361

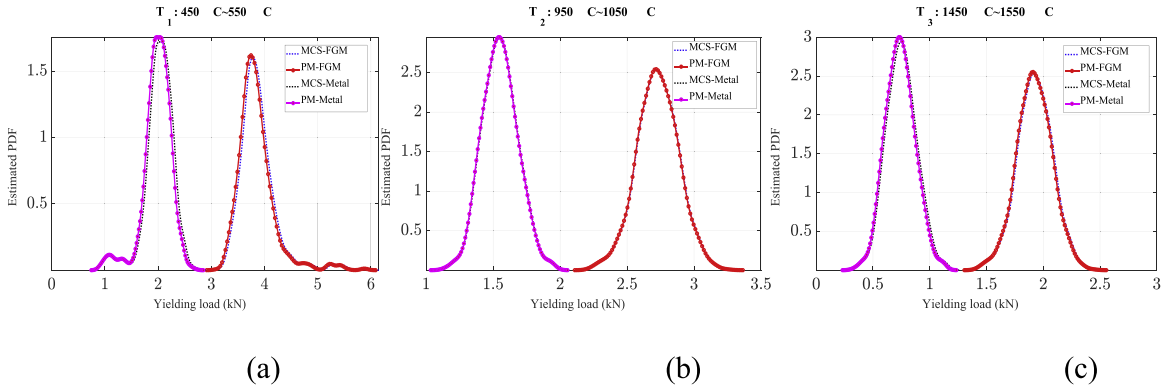

Fig. 14. The estimated PDFs of yielding load from FGM and pure metal at temperature ranges of (a) 450°~550°, (b) 950°~1050°, and (c) 1450°~1550°.

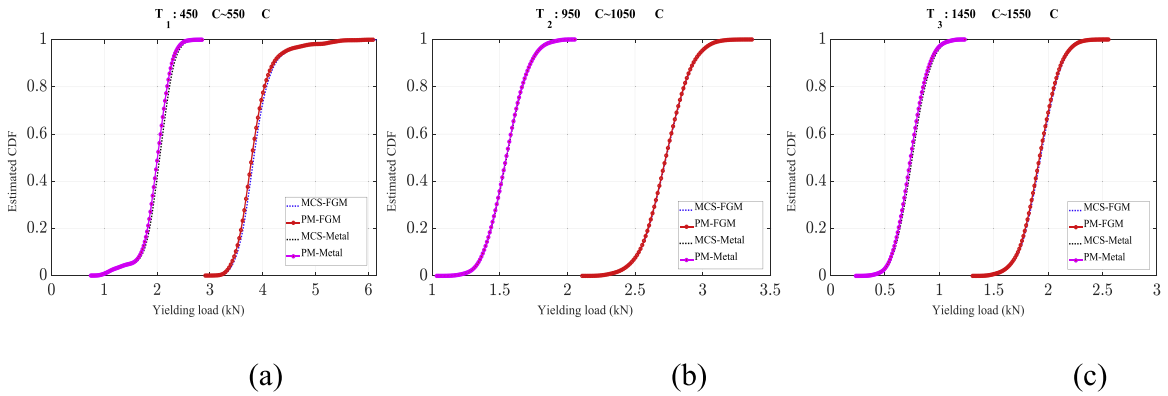

Fig. 15. The estimated CDFs of yielding load from FGM and pure metal at temperature ranges of (a) 450°~550°, (b) 950°~1050°, and (c) 1450°~1550°.

intervals. For instance, in temperature range 950°~1050°, the yielding load range of FGM block is from 2.1 kN to 3.4 kN, while for the pure metal block, the load range is from 1.0 kN to 2.1 kN. Also, the yielding displacement range of FGM block is from 0.04 cm to 0.16 cm, for pure metal is from 0.01 cm to 0.07 cm. From this case, it shows that FGM component has larger bearing load capacity and higher yielding deformation under high temperature working conditions, which is a significant improvement of mechanical behaviour compared to traditional homogeneous metallic component. Moreover, by using the virtual modelling technique, the nonlinear responses of both materials have been efficiently predicted under different thermal cases: total of 52.5 hours for 270 random samples running, 0.36 hour for virtual model training and establishment, and 2 minutes for yielding load and displacement predictions of both FGM engine block and pure metal block.

Detailed statistical moments about random yielding loads and displacements under three different temperature ranges for both materials are provided in Tables 7, 8. It has been clearly shown in the tables that the proposed method generate yielding loads of both FGM and metal components that simulates very close to the deterministic MCS responses. Accurate prediction results have also been observed for the estimated yielding displacement between two approaches for both components. Therefore, the accuracy, applicability and efficiency of the proposed framework has been once again reinforced through both PDF, CDF plots and statistical moment figures for traditional metallic materials and newly developed FGM structures.

As highlighted, one of the critical advantages of virtual modelling technique is the quick response prediction of structures against future random information. To illustrate this capability, in Table 9, a total of four groups of arbitrary generated random vectors are

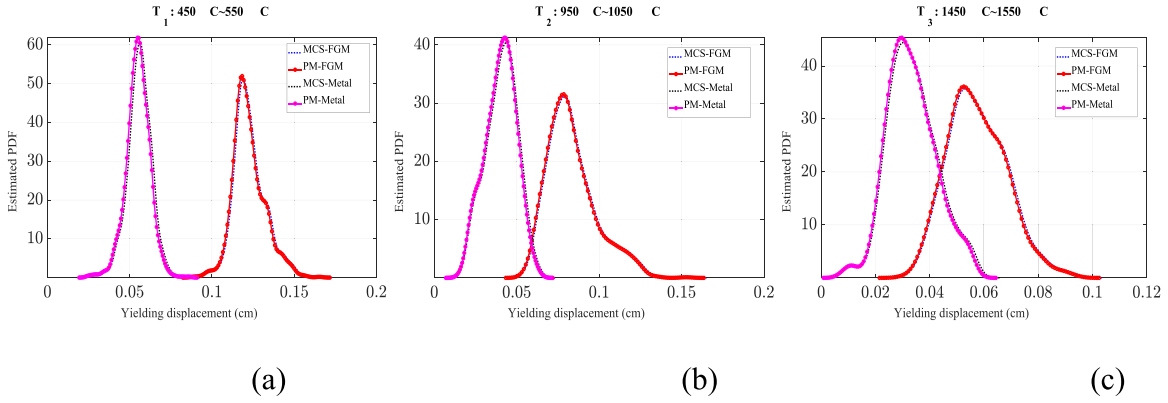

Fig. 16. The estimated PDFs of yielding displacement from FGM and pure metal at temperature ranges of (a) 450°~550°, (b) 950°~1050°, and (c) 1450°~1550°.

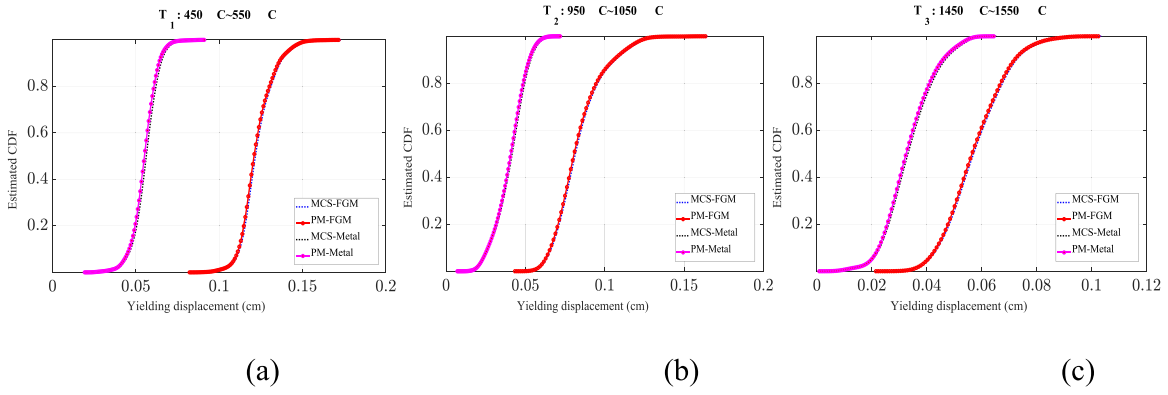

Fig. 17. The estimated CDFs of yielding displacement from FGM and pure metal at temperature ranges of (a) 450°~550°, (b) 950°~1050°, and (c) 1450°~1550°.

Table 7
The estimated moments of yielding load at different temperature ranges.

Temperature range	Moments	Methods	Yielding load	
			FGM	Metal
T_1	Mean (kN)	PM	3.843	2.076
		MCS	3.841	2.077
	Standard deviation	PM	1.673	1.739
		MCS	1.672	1.736
T_2	Mean (kN)	PM	2.764	1.633
		MCS	2.759	1.631
	Standard deviation	PM	1.883	1.905
		MCS	1.879	1.908
T_3	Mean (kN)	PM	1.865	0.731
		MCS	1.860	0.727
	Standard deviation	PM	2.174	2.269
		MCS	2.181	2.261

provided to be considered as structural inputs. By using the already developed virtual models of both FGM engine block and pure metal block, the deterministic FE simulation process can be avoided and the four groups of random inputs can be directly substituted into the explicit virtual model formulations to acquire the structural responses. Detailed prediction results of both components have been provided in Figs. 18, 19. As shown in Figs. 18, 19, it is evident that under different input information, the predicted nonlinear responses of both FGM and metal blocks from virtual models are almost identical with the actual deterministic results, even considering different temperature levels. The maximum relative error between these two approaches is smaller than 2%, which is acceptable in practical engineering field. In the meantime, considering the continuously varied information in real-life thermal environmental working

Table 8
The estimated moments of yielding displacement at different temperature ranges.

Temperature range	Moments	Methods	Yielding displacement	
			FGM	Metal
T_1	Mean (cm)	PM	0.127	0.0675
		MCS	0.126	0.0673
	Standard deviation	PM	0.983	1.031
		MCS	0.981	1.034
T_2	Mean (cm)	PM	0.0763	0.0421
		MCS	0.0760	0.0417
	Standard deviation	PM	1.258	1.167
		MCS	1.262	1.159
T_3	Mean (cm)	PM	0.0561	0.0272
		MCS	0.0558	0.0266
	Standard deviation	PM	1.573	1.671
		MCS	1.568	1.665

Table 9
Arbitrary generated FGM structural random inputs.

System phase	Material property	Case I	Case II	Case III	Case IV
Metal	E_m (GPa)	206	224	218	235
	υ_m	0.23	0.25	0.22	0.28
	σ_Y (MPa)	210	215	207	229
	κ_m	810.1	803.5	823.6	800.3
	ρ_m (kg/m^3)	6340	6295	6488	6216
	α_m (10^{-6}/°C)	7.55	8.01	8.12	7.47
Ceramic	E_c (GPa)	154	163	172	164
	υ_c	0.21	0.24	0.26	0.27
	ρ_c (kg/m^3)	3122	3245	3301	3005
	α_c (10^{-6}/°C)	5.06	5.23	5.44	4.99
Temperature	T (°C)	468	546	1023	1534

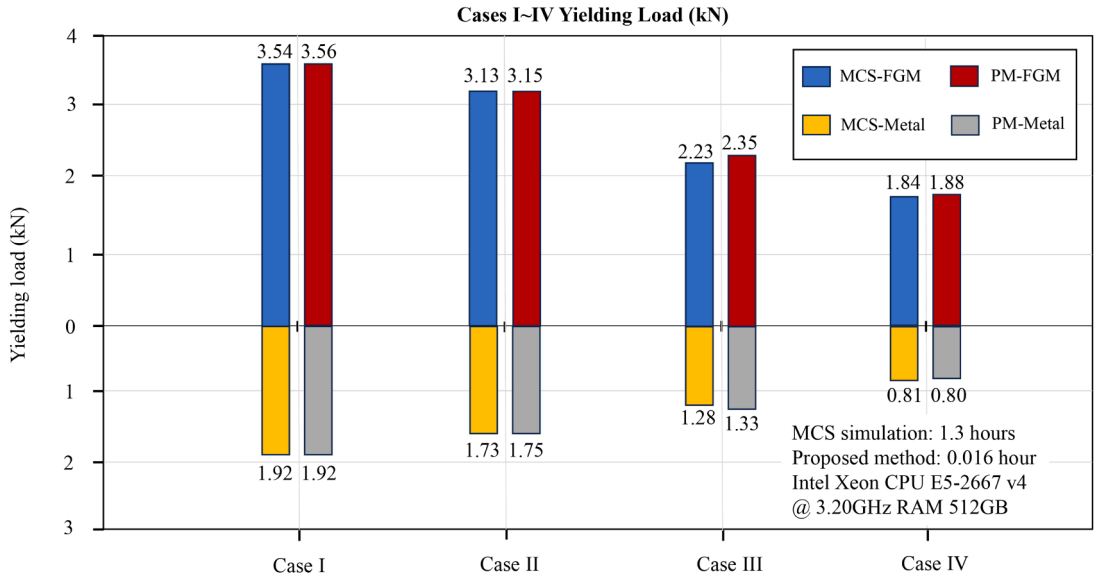

Fig. 18. Predicted yielding load of FGM engine block at random structural inputs.

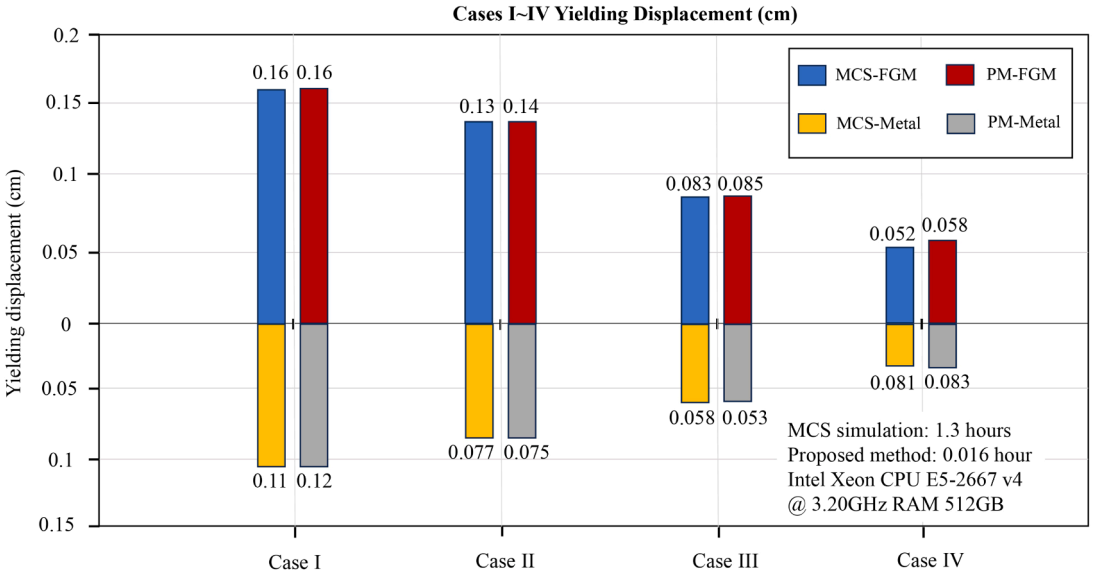

Fig. 19. Predicted yielding displacement of FGM engine block at random structural inputs.

conditions, the proposed virtual modelling technique for advanced FGM structure reduces a significant number of computational efforts in model analysis, safety/reliability evaluation and component inspection/maintenance disciplines.

6. Conclusion

In this study, the random elastoplastic analysis of functionally graded structures under high-temperature conditions is investigated. A novel thermal-mechanical coupling framework, termed thermoplastic-virtual model, is proposed by incorporating temperature dependent performance, hardening plastic behaviour and artificial intelligence technique within one unified system. The Touloukian and Tamura-Tomota-Ozawa models are employed to simulate the high temperature effects and nonlinear material behaviours of the FG structure, respectively. In addition, to ensure a robust and physically feasible high temperature induced stochastic elastoplastic analysis, an extended support vector regression based virtual modelling approach is introduced for multivariate uncertainty quantification. Such that the deformed nonlinear deflection, plastic damage zone, and fragility curves could be directly estimated through established surrogate model for FG structure under various temperature distributions. This approach enables the effective estimation of statistical characteristics of any concerned structural nonlinear responses. Consequently, the performance of the FG structure against both serviceability and strength limit states under high-temperature conditions can be thoroughly assessed. The effectiveness, accuracy, and applicability of the proposed thermal-plastic virtual model are fully demonstrated through the detailed investigation of two practical FG structures, which can be critical and referrable for high temperature involved elastoplastic deformation prediction of real-life composite structures.

Additionally, Poisson's ratio in this research is prescribed as a spatially and thermally varying function for analytical convenience. However, the author acknowledges that Poisson's ratio enters the constitutive relations nonlinearly and cannot be reliably interpolated between constituent values using classical mixture rules. To maintain internal consistency for isotropic materials, the shear modulus is not independently defined but derived using the relation $G(\boldsymbol{x},\mathrm{T}) = E(\boldsymbol{x},\mathrm{T})/[1 - 2\cdot\upsilon(\boldsymbol{x},\mathrm{T})]$. While this approach is mathematically consistent, it may not reflect physically homogenized behaviour. More rigorous treatment using micromechanical models is prepared for future work.

CRediT authorship contribution statement

Yuan Feng: Writing – original draft, Software, Methodology, Investigation, Formal analysis, Conceptualization.

Declaration of competing interest

The authors declare that they have no known competing financial interests or personal relationships that could have appeared to influence the work reported in this paper.

Acknowledgements

The research work has been undertaken with the assistance of resources and services from the National Computational

Infrastructure (NCI) Australia.

Appendix A. Formulations of vectors and matrix defined in the optimization problem

The vectors and matrices of $\widehat{Q}_x$, $\widehat{A}_x$, $\widehat{D}_x$, a_x^T, $\widehat{\mathbf{e}}_x$, $\widehat{\mathbf{k}}_x$ and r_x involved within the X-SVR optimization expression can be presented by:

$$\widehat{\mathbf{Q}}_x = \begin{bmatrix} \gamma_1\mathbf{I}_{j\times j} & & & \\ & \gamma_1\mathbf{I}_{j\times j} & & \\ & & p\mathbf{I}_{i\times i} & \\ & & & p\mathbf{I}_{i\times i} \end{bmatrix}, \widehat{\mathbf{A}}_x = \begin{bmatrix} \mathbf{0}_{2j\times 2j} & \mathbf{0}_{2j\times i} & \mathbf{0}_{2j\times i} \\ \mathbf{0}_{i\times 2j} & \mathbf{I}_{i\times i} & \mathbf{0}_{i\times i} \\ \mathbf{0}_{i\times 2j} & \mathbf{0}_{i\times i} & -\mathbf{I}_{i\times i} \end{bmatrix}, \widehat{\mathbf{D}}_x = \begin{bmatrix} \mathbf{0}_{2j\times j} & \mathbf{0}_{2j\times j} & \mathbf{0}_{2j\times 2i} \\ -\mathbf{x}_{train} & \mathbf{x}_{train} & \mathbf{0}_{i\times 2i} \\ \mathbf{x}_{train} & -\mathbf{x}_{train} & \mathbf{0}_{i\times 2i} \end{bmatrix} \tag{A1}$$

$$\mathbf{a}_x = \begin{bmatrix} \mathbf{e}_j \\ \mathbf{e}_j \\ \mathbf{0}_{2i} \end{bmatrix}, \quad \widehat{\mathbf{e}}_x = \begin{bmatrix} \mathbf{0}_{2j} \\ \mathbf{e}_i \\ \mathbf{e}_i \end{bmatrix}, \quad \widehat{\mathbf{k}}_x = \begin{bmatrix} \mathbf{0}_{2j} \\ \mathbf{y}_{train} \\ -\mathbf{y}_{train} \end{bmatrix}, \quad \mathbf{r}_x = \begin{bmatrix} \mathbf{p}_x \\ \mathbf{q}_x \\ \vartheta \\ \widehat{\vartheta} \end{bmatrix} \tag{A2}$$

Data availability

No data was used for the research described in the article.

References

[1] R.M. Mahamood, E.T. Akinlabi, Types of functionally graded materials and their areas of application, Top. Min. Met. Mater. Eng. (2017) 9–21.
[2] S. Chandrasekaran, S. Hari, M. Amirthalingam, Functionally graded materials for marine risers by additive manufacturing for high-temperature applications: Experimental investigations, Structure 35 (2022) 931–938.
[3] Aircraft serious incident investigation report. (2024). https://www.mlit.go.jp/jtsb/eng-air_report/N645NW.pdf.
[4] A. Abid, M.T. Sarowar, Heat transfer, thermal stress and failure inspection of a gas turbine compressor stator blade made of five different conventional superalloys and ultra-high-temperature ceramic material: a direct numerical investigation, J. Fail. Ana. Prev. 22 (3) (2022) 878–898.
[5] B. Dong, Y. Yu, Y. Feng, D. Wu, G. Zhao, A. Liu, W. Gao, Robust numerical solution for assessing corrosion of reinforced concrete structures under external power supply, Eng. Struct. 294 (2023) 116724.
[6] C. Lee, G. Kim, Y. Chou, B.L. Musicó, M.C. Gao, K. An, G. Song, Y.C. Chou, V. Keppens, W. Chen, P.K. Liaw, Temperature dependence of elastic and plastic deformation behavior of a refractory high-entropy alloy, Sci. Adv. 6 (37) (2020).
[7] C. Arndt, C. Crusenberry, B. Heng, R. Butler, S. TerMaath, Reduced-Dimension surrogate modeling to characterize the damage tolerance of composite/metal structures, Model 4 (4) (2023) 485–514.
[8] Z. Zhang, D. Zhou, H. Fang, J. Zhang, X. Li, Analysis of layered rectangular plates under thermo-mechanical loads considering temperature-dependent material properties, Appl. Math. Model. 92 (2021) 244–260.
[9] X. Yao, H. Shao, D. Wang, X. Wei, A general thermo-elastoplastic constitutive theory for thermal-sensitive materials with temperature-dependent properties, Appl. Math. Model. 132 (2024) 319–341.
[10] R.W. Hertzberg, R.P. Vinci, J.L. Hertzberg, Deformation and Fracture Mechanics of Engineering Materials, John Wiley & Sons, Inc, 2021.
[11] Y. Feng, D. Wu, L. Liu, W. Gao, F. Tin-Loi, Safety assessment for functionally graded structures with material nonlinearity, Struct. Saf. 86 (2020) 101974.
[12] Y.S. Li, B.L. Liu, Thermal buckling and free vibration of viscoelastic functionally graded sandwich shells with tunable auxetic Honeycomb Core, Appl. Math. Model. 108 (2022) 685–700.
[13] C. Tao, T. Dai, Analyses of thermal buckling and secondary instability of post-buckled S-FGM plates with porosities based on a Meshfree method, Appl. Math. Model. 89 (2021) 268–284.
[14] Z. Zhang, D. Zhou, Y.M. Lim, H. Fang, R. Huo, Analytical solutions for multilayered pipes with temperature-dependent properties under non-uniform pressure and thermal load, Appl. Math. Model. 106 (2022) 369–389.
[15] Y. Sitli, K. Mhada, O. Bourihane, H. Rhanim, Buckling and post-buckling analysis of a functionally graded material (FGM) plate by the asymptotic numerical method, Structure 31 (2021) 1031–1040.
[16] M. Saad, L. Hadji, Thermal buckling analysis of porous FGM plates, Mater. Today Proc. 53 (2022) 196–201.
[17] R. Kumar, V.S. Kumar, M.M. Butt, N.A. Sheikh, S.A. Khan, A. Afzal, Thermo-mechanical analysis and estimation of turbine blade tip clearance of a small gas turbine engine under transient operating conditions, Appl. Ther. Eng. 179 (2020) 115700.
[18] Y. Tian, Q. Li, Y. Feng, Y. Yu, D. Wu, X. Chen, W. Gao, Nonlinear dynamic analysis of the functionally graded graphene platelets reinforced porous plate under moving mass, Thin-Walled Struct. 183 (2023) 110363.
[19] A. Carvalho, T. Silva, M.A. Loja, F.R. Damásio, Assessing the influence of material and geometrical uncertainty on the mechanical behavior of functionally graded material plates, Mech. Adv. Mater. Struct. 24 (5) (2016) 417–426.
[20] M. Khayat, A. Baghlani, M.A. Najafgholipour, A hybrid algorithm for modeling and studying of the effect of material and mechanical uncertainties on stability of sandwich FGM materials under thermal shock, Compos. Struct. 293 (2022) 115657.
[21] S.S. Tomar, M. Talha, Influence of material uncertainties on vibration and bending behaviour of skewed sandwich FGM plates, Compos. B Eng. 163 (2019) 779–793.
[22] J. Xie, P. Shi, H. Li, F. Li, Thermomechanical problem of functionally graded spherical shells based on homogenization schemes: Data-driven volume fraction optimization with material uncertainties, Appl. Math. Model. 131 (2024) 103–133.
[23] R. Baghlani, M.A. Najafgholipour, M. Khayat, The influence of mechanical uncertainties on the free vibration of functionally graded graphene-reinforced porous nanocomposite shells of revolution, Eng. Struct. 228 (2021) 111356.
[24] V.H. Truong, T.S. Cao, S. Tangaramvong, A robust machine learning-based framework for handling time-consuming constraints for bi-objective optimization of nonlinear steel structures, Structure 62 (2024) 106226.
[25] T. Van Huynh, S. Tangaramvong, B. Do, W. Gao, S. Limkatanyu, Sequential most probable point update combining Gaussian process and comprehensive learning PSO for structural reliability-based design optimization, Reliab. Eng. Syst. Saf. 235 (2023) 109164.
[26] M. Kolev, Predictive analysis of mechanical properties in Cu-Ti alloys: a comprehensive machine learning approach, Model 5 (3) (2024) 901–910.

[27] P.K. Karsh, T. Mukhopadhyay, S. Dey, Stochastic investigation of natural frequency for functionally graded plates, IOP Conf. Ser. Mater. Sci. Eng. 326 (2018) 012003.
[28] V.S. Chandel, M. Talha, The random thermo-elastic nonlinear vibration analysis of porous FGM nano-beams using the first order perturbation theory, Proc. Inst. Mech. Eng. C J. Mech. Eng. Sci. 238 (11) (2023) 5241–5257.
[29] V.D. Quang, N.D. Khoa, N.D. Duc, The effect of structural characteristics and external conditions on the dynamic behavior of shear deformable FGM porous plates in thermal environment, J. Mech. Sci. Tech. 35 (8) (2021) 3323–3329.
[30] M. Bakhtiari, M. Kheradpisheh, Dynamics behavior and imperfection sensitivity of a fluid-filled multilayered FGM cylindrical structure, Int. J. Mech. Sci. 176 (2020) 105425.
[31] Y. Cai, L. Li, X. Lv, H. Chen, X. Fan, An analytical approach for out-of-plane vibration of Timoshenko thin-walled curved beam with a mono-symmetric cross-section under a moving mass, Appl. Math. Model. 136 (2024) 115633.
[32] K. Hejranfar, K. Parseh, Numerical simulation of structural dynamics using a high-order compact finite-difference scheme, Appl. Math. Model. 40 (3) (2016) 2431–2453.
[33] V.H. Truong, H.A. Pham, T.H. Van, S. Tangaramvong, Evaluation of machine learning models for load-carrying capacity assessment of semi-rigid steel structures, Eng. Struct. 273 (2023) 115001.
[34] Y. Feng, Q. Wang, X. Chen, D. Wu, W. Gao, Virtual modelling technique for geometric-material nonlinear dynamics of structures, Struct. Saf. 100 (2023) 102284.
[35] Y. Feng, Q. Wang, Y. Yu, T. Zhang, D. Wu, X. Chen, Z. Luo, W. Gao, Experimental-numerical-virtual (ENV) modelling technique for composite structure against low velocity impacts, Eng. Struct. 278 (2023) 115488.
[36] Y. Tian, Q. Li, Y. Feng, Z. Luo, D. Ruan, W. Gao, Nonlinear dynamic analysis of the graphene platelets reinforced porous plate with magneto-electro-elastic sheets subjected to impact load, Non Dyn. 112 (3) (2023) 1661–1690.
[37] Y. Feng, M.M. Alamdari, D. Wu, Z. Luo, D. Ruan, T. Egbelakin, X. Chen, W. Gao, Virtual modelling aided safety assessment for ductile structures against high-velocity impact, Eng. Struct. 301 (2024) 117373.
[38] Z. Shi, Y. Feng, M.G. Stewart, W. Gao, Virtual modelling-based fragility assessment of structures under bushfire propagation, Reliab. Eng. Syst. Saf. 245 (2024) 110000.
[39] Y. Liu, Y. Feng, D. Wu, X. Chen, W. Gao, Virtual modelling integrated phase field method for dynamic fracture analysis, Int. J. Mech. Sci. 252 (2023) 108372.
[40] Y.S. Touloukian, T.P.R. Center, Thermophysical Properties of High Temperature Solid Materials. Vol. 1. Elements. Pt. 1, Macmillan, 1967.
[41] J.N. Reddy, C.D. Chin, Thermomechanical analysis of functionally graded cylinders and plates, J. Trauma. Stress 21 (1998) 593–626.
[42] I. Tamura, Y. Tomota, H. Ozawa, Strength and ductility of Fe-Ni-C alloys composed of austenite and martensitewith various strength, in: Proceedings of the 3rd Conference on Strength of Metals and Alloys, Cambridge, 1973, pp. 611–615.
[43] M. Koizumi, FGM activities in Japan, Compos. B Eng. 28 (2002) 1–4.
[44] A.K. Soh, L.C. Bian, J. Chakrabarty, Elastic/plastic buckling of a composite flat plate subjected to uniform edge compression, Thin-Walled Struct. 38 (2000) 247–265.
[45] S. Suthaharan, Support vector machine, S. Suthaharan (Ed.). Machine Learning Models and Algorithms for Big Data Classification: Thinking with Examples for Effective Learning, Springer US, Boston, MA, 2016, pp. 207–235.
[46] Y. Bazilevs, V.M. Calo, J.A. Cottrell, J.A. Evans, T.J.R. Hughes, S. Lipton, T.W. Sederberg, Isogeometric analysis using T-splines, Comput. Methods Appl. Mech. Eng. 199 (5) (2010) 229–263.
[47] M. Navarro-García, V. Guerrero, M. Durban, On constrained smoothing and out-of-range prediction using P-splines: a conic optimization approach, Appl. Math. Comput. 441 (2023) 127679.
[48] X. Li, T.W. Sederberg, S-splines: a simple surface solution for IGA and CAD, Comput. Methods Appl. Mech. Eng. 350 (2019) 664–678.

Dr. Yuan Feng is a Marie Skłodowska-Curie Action Fellow of the European Commission, and Research Fellow at University of Technology Sydney. He received his B.E from Northwest A & F University in 2015, M.E from Harbin Institute of Technology in 2017, and Ph.D. from UNSW, Sydney in 2021. He has successfully secured an Early Career Researcher funding through National Computational Infrastructure, Dean...s Award for Outstanding PhD Theses and participated in 4 ARC Discovery projects. His research focuses on engineering risk assessment and probabilistic methods for infrastructure systems, leveraging machine learning to enhance reliability analysis and understanding complex system behavior.